



ELSEVIER

Spectrochimica Acta Part B 56 (2001) 487–501

SPECTROCHIMICA  
ACTA  
PART B

www.elsevier.nl/locate/sab

# Spectral, spatial and temporal characterization of a millisecond pulsed glow discharge: copper analyte emission and ionization

Cris L. Lewis<sup>a</sup>, Glen P. Jackson<sup>a</sup>, Stephen K. Doorn<sup>b</sup>, Vahid Majidi<sup>b</sup>,  
Fred L. King<sup>a,\*</sup>

<sup>a</sup>Department of Chemistry, West Virginia University, P.O. Box 6045, Morgantown, WV 26505-6045, USA

<sup>b</sup>Los Alamos National Laboratory, Chemistry Division, MS K484, Los Alamos, NM 87545, USA

Received 24 June 2000; accepted 5 March 2001

## Abstract

Two-dimensional maps of the spatial distributions of excited and ionized sputtered copper atoms are presented for a millisecond pulsed argon glow discharge. These maps demonstrate the temporal as well as spatial dependence of different excitation and ionization processes over the pulse cycle. Transitions from the low energy electronic states for the atom, characterized by emission such as that at 324.75 nm (3.82 → 0.00 eV), dominate the plateau time regime at a distance of 2.5 mm from the cathode surface. These processes originate from the electron excitation of ground state copper atoms. Transitions from high-energy electronic states, such as that characterized by emission at 368.74 nm (7.16 → 3.82 eV), predominate during the afterpeak time regime at a distance of 5.0–6.0 mm from the cathode surface. This observation is consistent with the relaxation of highly excited copper atoms produced by electron recombination with copper ions during the afterpeak time regime. Analyses of afterpeak and plateau intensities for a series of copper emission lines indicate an electron excitation temperature equivalent to 5.78 eV at 0.8 torr and 1.5 W. Temporal profiles exhibit copper ion emission only during the plateau time regime. © 2001 Elsevier Science B.V. All rights reserved.

**Keywords:** Pulsed glow discharge; Optical spectrometry; Excitation and ionization; Mechanisms; Plasma processes

\* Corresponding author. Tel.: +1-304-293-3435, ext. 4451; fax: +1-304-293-4904.

E-mail address: fking@wvu.edu (F.L. King).

## 1. Introduction

Pulsed operation of the analytical glow discharge source affords unique analytical advantages as well as alleviating plasma instability arising from the resistive overheating of the sample cathode [1]. Such operation of pulsed glow discharge sources consists of an applied square wave power pulse followed by a period of power termination. The width of the applied power pulse may vary from several microseconds ( $\mu\text{s}$ ) to milliseconds (ms) at frequencies up to 100 Hz [2,3]. A principal analytical advantage is the creation of time regimes in which analyte signal is enhanced and background signal is suppressed. Time gated detection permits this advantage to be exploited.

Illustrations of the analytical utility of pulsed glow discharge sources coupled with time-gated mass spectrometric detection include: (1) the temporal resolution between signals of ions arising from the discharge working gases and that from sputtered analyte [4,5]; (2) and the determination of molecular weight and structure of volatile organic molecules [6]. These examples rely on the temporal characteristics of the dynamic gas phase reactions that occur in these pulsed glow discharge sources. The current work shows that further advantages may be gained from exploitation of the spatial characteristics of these plasmas as well.

A typical ms-pulsed glow discharge operating sequence includes an applied power pulse of 5 ms followed by power termination for 15 ms. During the 5-ms applied power pulse, gas phase species and sputtered species undergo a series of excitation and ionization processes. Of these processes, electron excitation and Penning ionization are dominant [7]. Upon power termination, the electron excitation process halts, as the plasma changes from an excitation/ionization mode to a recombination mode. In this recombination mode, thermal electrons and plasma ions recombine to produce excited and metastable atoms. At this time in the pulse cycle, the enhancement of the metastable argon atom population leads to an increase in Penning ionization [8]. This enhancement of Penning ionization not only leads to an increase in ionization of sputtered atoms but also

leads to an increase in emission from the sputtered atoms. Because of these enhancements in analyte signals, this ‘afterpeak’ time period is of great interest to the analyst [1].

This report relies on a series of optical investigations of ms-pulsed glow discharge sources to elucidate the processes leading to the afterpeak signal. The metastable argon atom population is found to vary temporally and spatially throughout the pulse cycle. During the plateau time regime, metastable production occurs primarily through electron excitation in the high potential field region near the cathode surface. At this time, and until power termination, the metastable argon atom population maximizes 1–2 mm from the cathode surface. Upon power termination, metastable argon atom production occurs primarily through recombination of argon ions with thermalized electrons. This population maximizes 0.3 ms after power termination and approximately 6 mm from the cathode surface [9]. The differences in sputtered analyte excitation and ionization mechanisms and their spatial as well as temporal separation are the focus of the studies reported here.

## 2. Experimental

Detailed descriptions of the glow discharge source and optical spectrometry system employed here appear in previous papers [3,9]. The glow discharge operated at a pulse rate of 50 Hz with a 25% duty cycle and an instantaneous applied power level of 1.5 W. The operating pressure was maintained at 0.8 torr with ultra pure argon gas (Airgas, Radnor, PA, USA). The glow discharge sample cathode consisted of a 4-mm diameter copper disk (SRM 495, NIST Gaithersburg, MD, USA) that was mounted on the end of a direct insertion probe. Vertical positioning was obtained through careful adjustment of the direct insertion probe with respect to the center of the discharge chamber; whereas, horizontal positioning was obtained by use of an *X–Y* positioning stage on which the glow discharge chamber was mounted.

Transient emission signals were recorded directly from the photomultiplier tube (Model R-

928, Hamamatsu, Japan) by a 1-GHz oscilloscope (9370M, LeCroy, Chestnut Ridge, NY, USA). Each digitized trace represented the summation of 100 discharge pulse cycles, each consisting of 2500 data points. Atomic absorbance measurements for copper species were collected using a copper-neon hollow cathode lamp operated at 16 mA. The lamp output was modulated at 3 kHz by

a mechanical chopper (197, EG & G PAR, Princeton, NJ, USA). The chopped beam was then focused through the glow discharge cell and plasma onto the entrance slit of the 0.64-m monochromator (ISA HR-640, Edison, NJ, USA). Both the entrance and exit slits were fixed at 50  $\mu\text{m}$ . Signal response from the photomultiplier tube was processed by a lock-in-amplifier (5210, EG & G

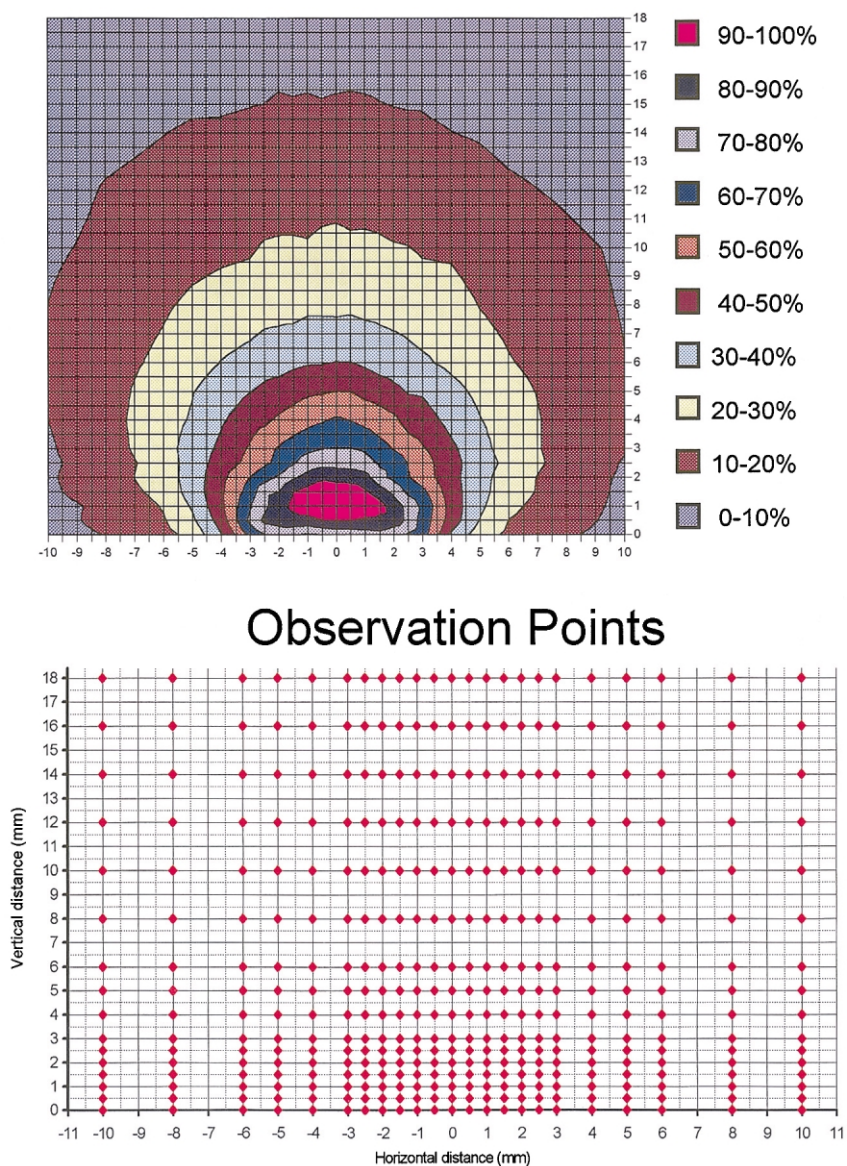


Fig. 1. Map legend and map spatial positions of the 368 observations. Scale is 0–100% of its emission or absorbance maximum.

PAR, Princeton, NJ, USA) tuned to the chopper frequency. An oscilloscope was used to monitor the temporal output from the LIA and to digitize the resulting data.

Measurements of the ground state copper atom population were accomplished by monitoring the absorption of 324.75-nm emission from the hollow cathode lamp. Deconvolution of the 1-ms LIA time constant was accomplished, using a low pass filter approximation and a series of Fourier transforms, inside of a spreadsheet program (Excel, Microsoft, Seattle, WA, USA) [10]. Following deconvolution, the data were baseline corrected and smoothed by repetitive moving averages of 10 points. The resultant digitized emission and deconvoluted absorbance traces were used to construct spatial maps of the glow discharge plasma consisting of such measurements collected at 368 spatial positions throughout the plasma, Fig. 1.

### 3. Results and discussion

#### 3.1. Copper atom transitions explored

These studies examine the temporal behavior for a series of copper atom transitions at increasing spatial distances from the cathode in the negative glow. Each series of electronic transitions demonstrates the characteristic plateau and afterpeak behavior described in previous papers [3]. In general, plateau intensities maximize 2.5–3.0 ms into the pulse cycle. At this time, and until power termination, the glow discharge exhibits a steady-state behavior as if it were not being pulsed. This steady-state behavior indicates the establishment of pseudo-equilibrium between excitation, de-excitation, and recombination processes. When power is terminated, plasma processes are dominated by the recombination of analyte and discharge gas ions with thermalized electrons. The result of these recombination processes is the formation of excited or metastable atoms for both the analyte and discharge gas species. Thus, as stated previously, each copper atom transition measured exhibits an afterpeak, which is a surge in emission intensity approximately 0.3–0.6 ms after power termination. Be-

cause electron excitation is quenched at the end of the power pulse, the source of this emission is the recombination of copper ions with electrons followed by radiative decay.

Experimental data obtained for various copper atom electronic transitions for both plateau and afterpeak emission intensities are summarized in Table 1. This table, constructed using emission data taken at 6.0 mm from the cathode surface, is presented to be both illustrative and informative of typical results. The listed plateau intensity values in Table 1 consist of an average intensity taken 4.5–5.0 ms within the pulse cycle, whereas the afterpeak intensity values consist of an average taken 5.3–5.6 ms; approximately 0.4–0.5 ms after power termination. When calculated, the ratio of the afterpeak-to-plateau intensity was found to vary as a function of the high-energy electronic state and the spatial position in the negative glow. This behavior can be explained by considering the various mechanisms leading to the population of the high-energy electronic states during the plateau and afterpeak time regimes. Generalizations regarding a series of electronic states are inferred from the six electronic regions depicted in the energy level diagram illustrated in Fig. 2. The subsequent emissions originating from these six electronic states (Fig. 3) represent emission behavior over different spatial regions in the negative glow. The mechanisms of the populating and depopulating processes for these various levels appeared previously in Bogaerts and Gijbels steady state model [11].

#### 3.2. $\text{Cu}^{\circ} 3d^{10}4p-4s$

Emission at 327.40 nm (Fig. 3A) corresponds with the decay of the  $3d^{10}4p$  level to the atom ground state. This state occurs 3.79 eV above the atom ground state with a transition probability of  $1.37 \times 10^{-8} \text{ s}^{-1}$  [12]. The large plateau intensity value evident in the temporal profiles of Fig. 3A indicates that population of the  $3d^{10}4p$  level occurs predominantly through electron excitation. As previously mentioned, this plateau regime mimics steady state discharges. Emission throughout this temporal regime originates from species subject to electron excitation. The plateau inten-

Table 1

Copper atom plateau and afterpeak emission intensities taken at 6.0 mm from the cathode surface with the corresponding calculated afterpeak-to-plateau ratio and the transitions high ( $E_H$ ) and low ( $E_L$ ) energy levels

nm	Intensity (mV)			Levels (eV)	
	Plateau	Afterpeak	Ratio	$E_L$	$E_H$
223.85	1.92	12.22	6.36	1.64	7.18
249.22	7.48	7.13	0.95	0.00	4.97
261.84	9.26	25.67	2.77	1.39	6.12
282.44	37.31	61.33	1.64	1.39	5.78
307.38	4.44	5.89	1.33	1.39	5.42
309.40	11.20	17.21	1.54	1.39	5.39
319.41	9.62	11.57	1.20	1.64	5.52
324.75	419.32	521.14	1.24	0.00	3.82
327.40	269.29	341.30	1.27	0.00	3.79
327.98	27.30	38.09	1.40	1.64	5.42
329.28	35.88	45.85	1.28	1.39	5.15
333.79	40.35	60.99	1.51	1.39	5.10
338.54	2.36	13.67	5.78	3.79	7.45
341.40	2.95	27.33	9.27	3.82	7.45
348.16	4.84	39.97	8.25	3.79	7.35
351.18	11.33	83.73	7.39	3.82	7.35
353.04	23.75	40.02	1.69	1.64	5.15
365.42	14.09	110.75	7.86	3.79	7.18
368.74	18.13	184.69	10.19	3.82	7.18
382.50	0.03	5.50	20.32	3.79	7.03
386.18	2.24	10.81	4.84	3.82	7.03
406.32	57.04	366.80	6.43	3.82	6.87
448.04	4.76	18.12	3.81	3.79	6.55
510.55	84.60	112.64	1.33	1.39	3.82
515.32	109.17	325.09	2.98	3.79	6.19
521.82	170.75	500.75	2.93	3.82	6.19
570.02	7.12	0.98	1.64	3.82	
578.21	11.87	13.85	1.17	1.64	3.79
793.31	6.17	9.76	1.58	3.79	5.35
809.26	11.02	18.65	1.69	3.82	5.35

sity maximizes at a sampling distance of 2 mm from the cathode surface and decreases at greater distances. In contrast, the afterpeak emission maximum appears approximately 0.3 ms after power termination, and is not distinct until 4 mm from the cathode surface. Over the next 6 mm, the afterpeak intensity decreases steadily but at a lower rate than the plateau intensity. Because the power was terminated the most probable mechanism of populating this level at this distance is through recombination and radiative decay of higher energy states, most notably through the  $3d^{10} 5, 6$  and  $7d$  levels. The population of these levels will be discussed in Section 3.3

### 3.3.3 $Cu^{\circ} 3d^{10} 5, 6$ and $7$ levels

The electronic states (labeled in Fig. 3B–E), illustrate the effects of spatial and temporal position on emission intensity for electronic states of increasing energy. Each state decays into the  $3d^{10}4p$  level. The plateau intensity of each transition reaches an emission maximum within 2 mm of the cathode surface followed by a reduction in intensity at greater distances. This plateau spatial position coincides with the spatial maximum found in the  $3d^{10}4p-4s$  transition, with electron excitation of  $Cu^{\circ}$  being the primary mechanism. This electron excitation mechanism remains dominant until the plasma decays. During the afterpeak time regime, emission profiles increase to reach maxima at 5.3–5.5 ms, and 4–6 mm from the cathode surface. Upon power termination, thermalized electrons and copper ions recombine to produce highly excited copper atoms. These, once formed, radiatively decay to lower electronic states. This radiative relaxation cascade is the most probable mechanism by which the lower energy levels, such as the  $3d^{10}4p$ , are populated once electron excitation halts following the termination of discharge power. This is consistent with previous reports that indicate the most probable production mechanism for copper ions in the afterpeak to be Penning ionization [9].

### 3.4. $Cu^{\circ} 3d^9 4s 4p-3d^9 4s^2$

Emission originating from the radiative decay of  $3d^9 4s 4p$  states to the  $3d^9 4s$  metastable copper atom states exhibit temporal afterpeak broadening as compared to other transitions studied. The reported transition probability of the 333.79-nm emission line, depicted in Fig. 3F, is  $3.80 \times 10^5 \text{ s}^{-1}$  [12]. This transition clearly has a much longer lifetime compared to the transitions previously discussed. During the plateau time regime, the major mechanism of excitation is electron excitation; whereas, the afterpeak intensity likely results from the radiative relaxation cascade from more highly excited copper atoms. The plateau and afterpeak intensity exhibit spatial maxima similar to that noted for the other electronic

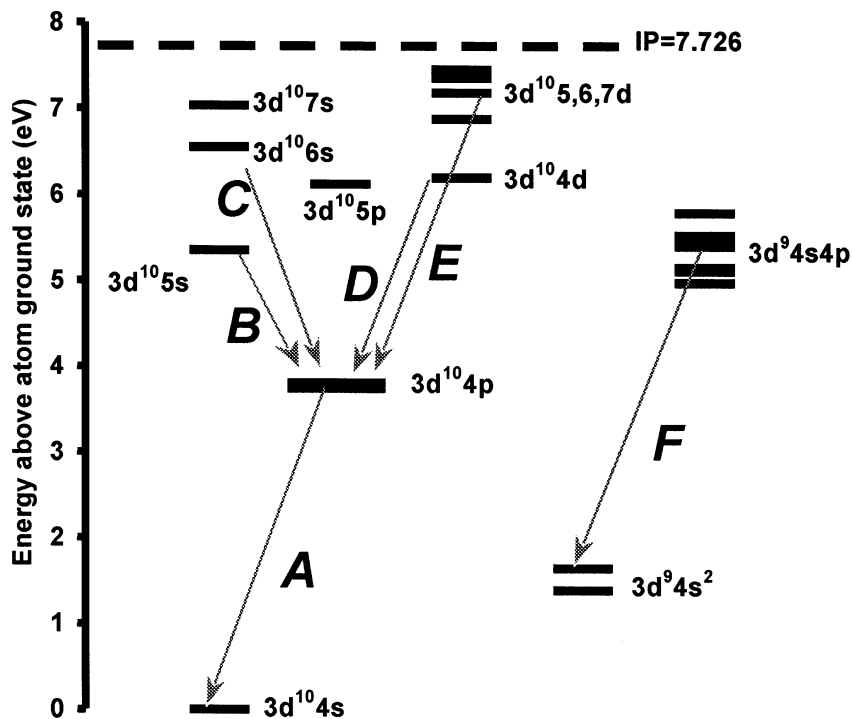


Fig. 2. Energy level diagram highlighting copper atom transitions of interest, labeled A–F (see Fig. 3).

states discussed above. The temporal broadening is attributed to the longer natural lifetime of 0.0026 ms, for this electronic state's decay to the copper atom metastable level.

### 3.5. Afterpeak-to-plateau emission intensity ratios

As alluded to in the above discussion, the ratio of copper atom afterpeak-to-plateau emission intensity increases with increasing energy of the upper electronic energy level. Fig. 4A is an illustration of this effect, where the ratio of afterpeak-to-plateau emission intensity is plotted as a function of the higher electronic energy level involved in a transition. This plot clearly shows that emission originating from higher electronic levels is heavily favored during the afterpeak time regime. Using the most intense transitions for various electronic levels observed, the ratio of afterpeak-to-plateau intensity is plotted as a function of distance (Fig. 4B). At shorter distances, during both plateau and afterpeak time regimes,

electron excitation dominates and the ratio is low. As distance increases, the ratio of afterpeak-to-plateau intensity increases with electronic energy levels. The most probable reason for this ratio increase is the production of copper ions by Penning ionization during the afterpeak time regime, followed by a loss in electron excitation. Plasma recombination processes in the afterpeak appear to maximize 6 mm from the cathode surface, this distance is needed for electrons to thermalize and fits well with the spatial position of metastable argon atom population maxima observed in this laboratory [9].

A closer inspection of Fig. 4B,C, reveals a distinct jump in the calculated afterpeak-to-plateau ratio moving between electronic states of 5.78 and 6.12 eV. The explanation for this jump is that the electron excitation temperature during the plateau has a mean value greater than 5.78 eV and less than 6.12 eV. This effect would limit the population of levels above 5.78 eV by electron excitation during the plateau time regime, leading

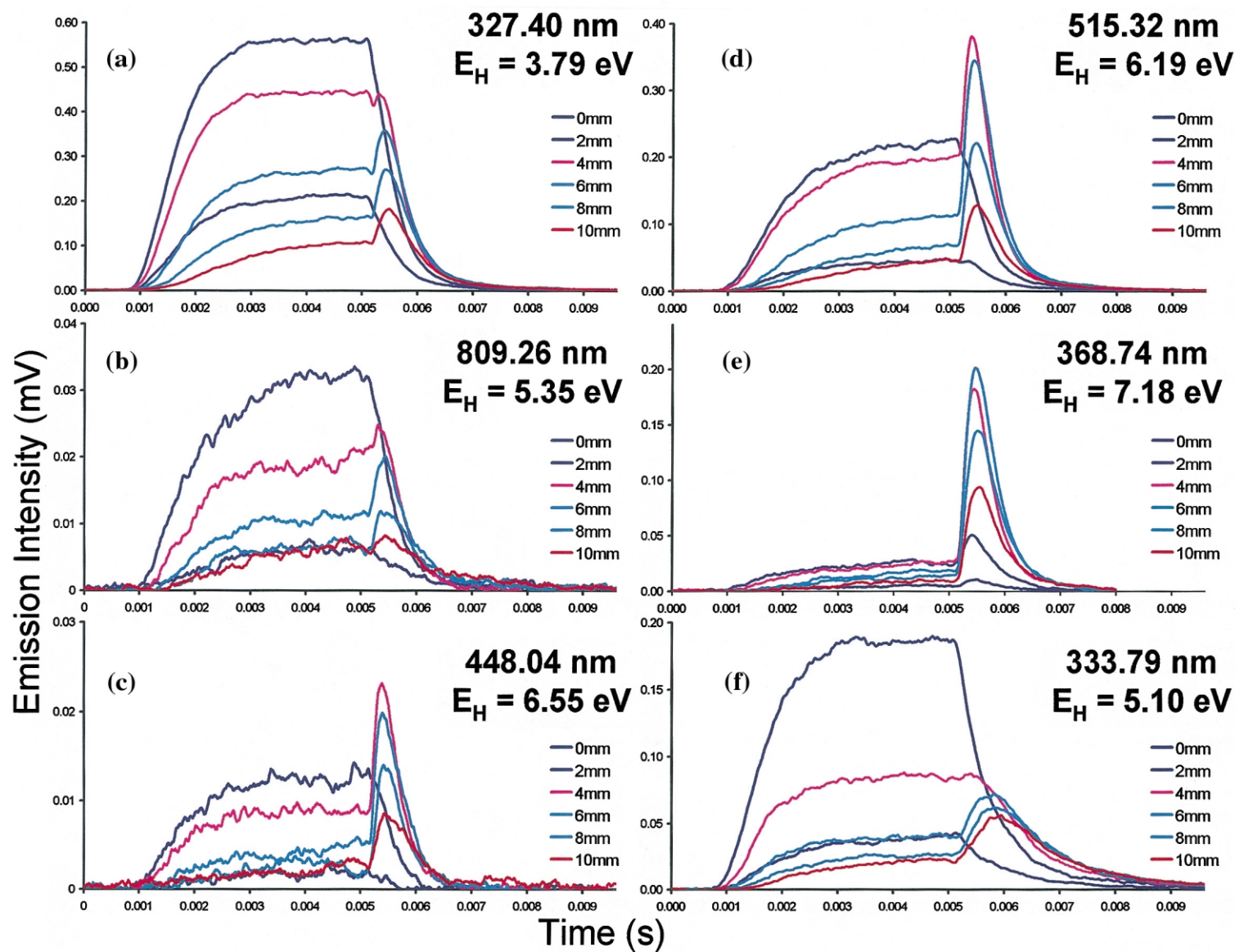


Fig. 3. The temporal emission profiles of copper atom transitions as depicted in Fig. 2, labeled A–F. Each transition demonstrates the change in the temporal emission profile moving vertically from the cathode surface in increments of 2 mm.

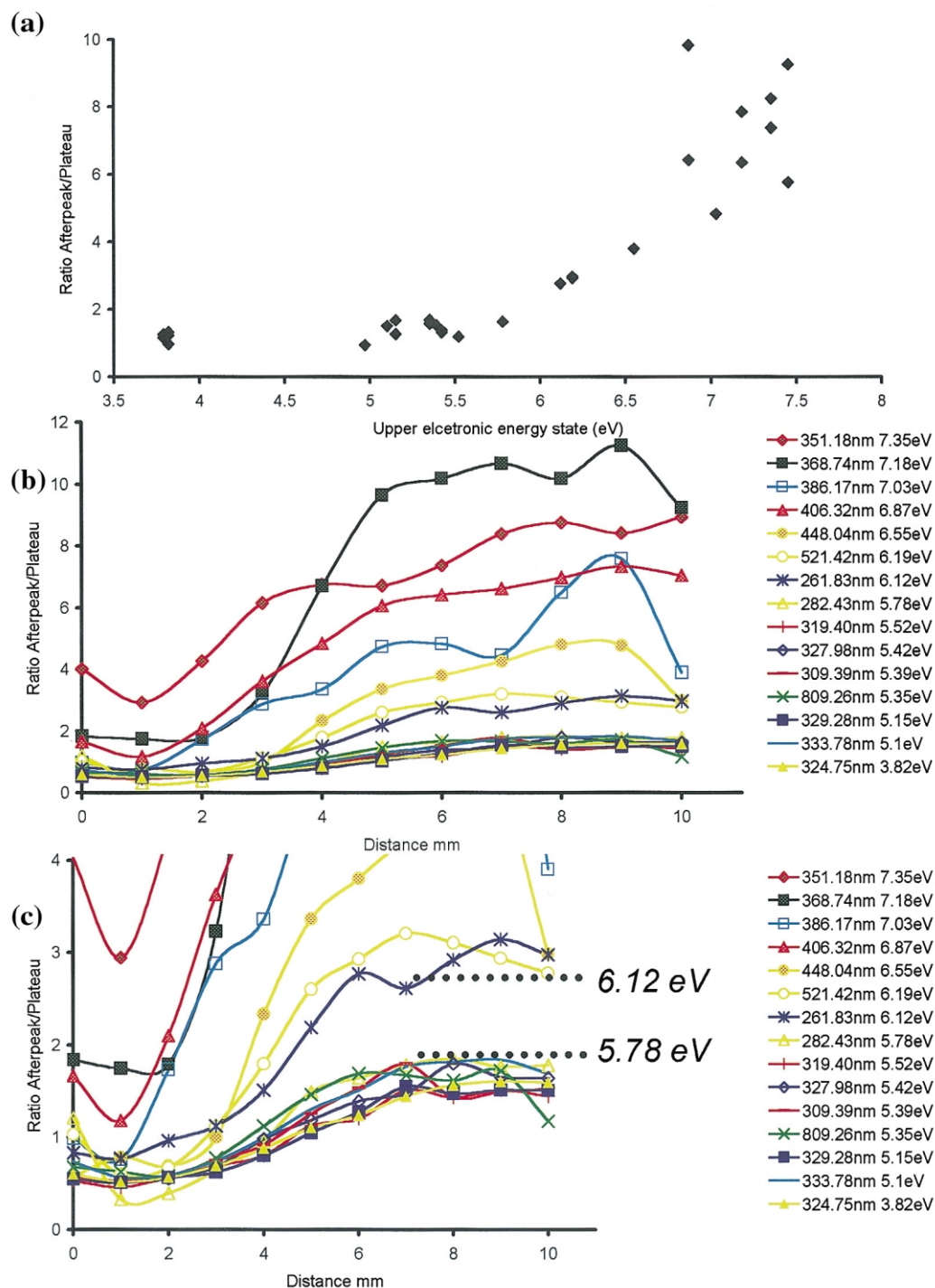


Fig. 4. Calculated afterpeak-to-plateau ratio as a function of increasing; (A) transition energy above the ground state at 6 mm; and (B) sampling distance above the cathode surface. Fig. 4C is an expanded view of Fig. 4B denoting a large jump in the calculated ratio.

to and increase in the calculated ratio. A previous report estimates electron temperatures in glow discharge plasmas to be on the order of 2–4 eV [13]. Future studies will examine the electron temperature inferred by this method for a variety of analyte materials.

#### 4. Spatial maps of atomic emission and absorbance of copper atoms

In order to show the relative positions and temporal responses of the differing emission processes more clearly, spatial maps of atomic emission and absorbance were collected under the same glow discharge conditions over a series of times in the pulse cycle. Each map consists of 368 spatial positions extending 10 mm laterally and 18 mm horizontally from the cathode's surface. The low and high-energy emission maps were selected based on intensity values and constructed by monitoring the emission from the 324.75 nm, 3.82 eV, and 368.74 nm, 7.12 eV transition, corresponding to emissions from the  $3d^{10}4p$  and  $3d^{10}6d$  electronic states.

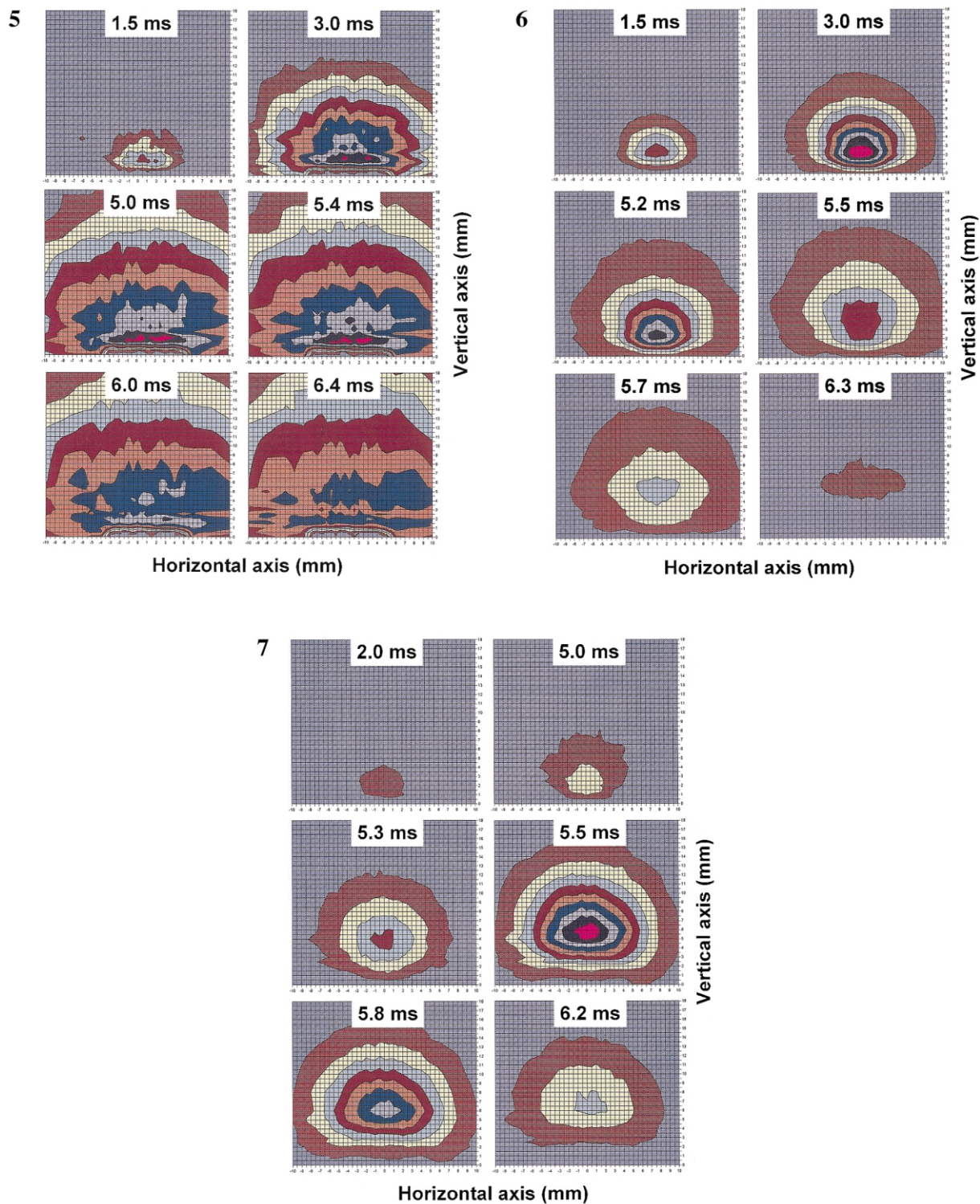
##### 4.1. Ground state copper atom absorbance maps

The maps in Fig. 5 illustrate the two-dimensional distribution of ground state copper atoms throughout the pulse cycle. The large rectangle of low absorbance extending 0.5 mm vertically and  $\sim 4$  mm horizontally from the origin is easily identifiable as the sample cathode and ceramic Macor shield. When power is applied, argon ions form through electron ionization and begin to sputter the cathode surface. At 1.5 ms into the pulse cycle the sputtering process has only just begun, over the next 3 ms the sputtered atom cloud extends outward, filling the glow discharge chamber. At this time a steady state population is reached that remains constant until 5.5 ms into the pulse cycle, 0.5 ms past power termination. During power application, the absorbance maximum is centered 1.5 mm above the edge of the cathode surface and radiates spherically outward. Each map exhibits a dip in absorbance intensity close to the cathode surface, which has been

observed in previous absorption, fluorescence and modeling studies [14–16]. As copper atoms sputter off the cathode surface they are subject to collisions with the argon bath gas. These collisions result in thermalization or a dampening of the initial kinetic energy that the sputtered atoms possessed upon leaving the cathode surface [17]. Once thermalized, the ground state copper atoms diffuse radially into the negative glow where they are subjected to collisional excitation and ionization processes. These maps demonstrate that a steady state population of copper atoms exists throughout the plateau and afterpeak time regime. Most notably, this shows that the spatial position of excitation and ionization of copper is not related to copper atom diffusion, but instead related to the diffusion of the ionizing/excitation collision partner, i.e. fast electron or metastable argon atom.

##### 4.2. Copper atom emission maps

The spatial and temporal responses of emission from the  $3d^{10}4p$  and  $3d^{10}6d$  electronic states are characterized in the maps shown in Figs. 6 and 7. The low-lying electronic state of  $3d^{10}4p$  is 3.82 eV above the copper atom ground state. In contrast, the  $3d^{10}6d$  electronic state is substantially higher at 7.18 eV. Each set of temporal maps is normalized to the highest intensity value during the pulse cycle for that particular transition, and relative changes to this maximum are reflected in multiples of 10% of its value. For both transitions the plateau intensity reaches a steady state value 3.0–4.0 ms into the pulse cycle. However, the relative intensity for each is quite different. At 3.0 ms into the pulse cycle the  $3d^{10}4p$  (3.82 eV) emission reaches 90–100% of its pulse cycle temporal maximum and extends radially outward. This emission sphere remains constant over the next 2.0 ms until 0.1 ms past power termination. Comparison with the  $3d^{10}6d$  (7.18 eV) emission, however, demonstrates a local maximum over the plateau regime that is only 20–30% of its temporal maximum. The relative positions of these two plateau maxima coincide with the edge of the ground state atom population observed in the previous absorption maps. As discussed in a pre-



Figs. 5–7.

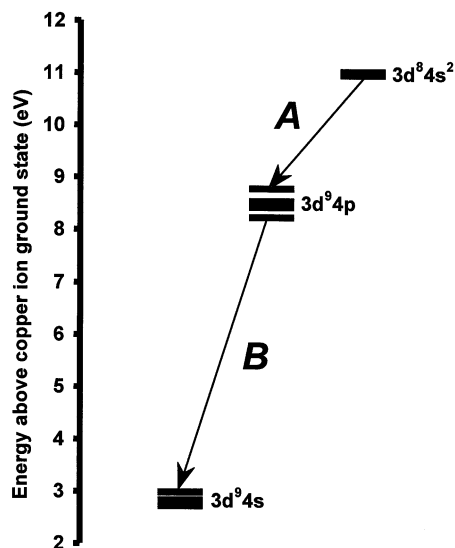


Fig. 8. Energy level diagram highlighting copper ion transitions of interest, labeled A–B (see Fig. 9).

vious section, electron excitation is the dominant excitation mechanism during the plateau time regime. Because of the relative magnitude of the energy states involved, electron excitation is the most probable mechanism for populating the  $3d^{10}4p$  (3.82 eV) electronic state. Populating the  $3d^{10}6d$  (7.18 eV) electronic state at this time through electron excitation would require an electron of significantly higher energy or multiple excitation steps.

Both temporal transition maps do not show significant changes in intensity until 5.1 ms into the pulse cycle. At this point, emission from the  $3d^{10}4p$  (3.82 eV) electronic state begins to decline from its temporal maximum. During this decline, the center of intensity shifts further away from the cathode into the negative glow. This change in position occurs over a 0.6-ms time period, with

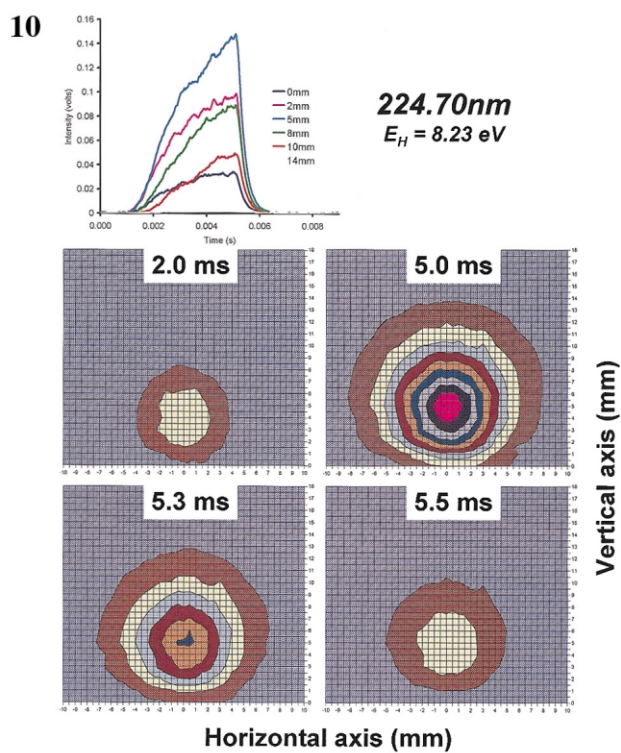
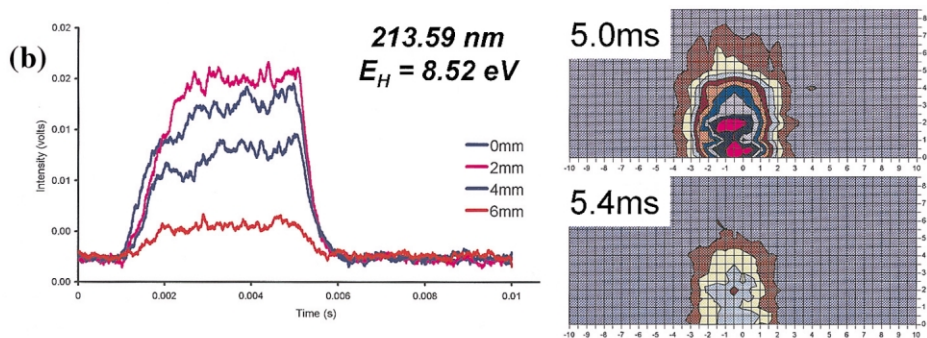
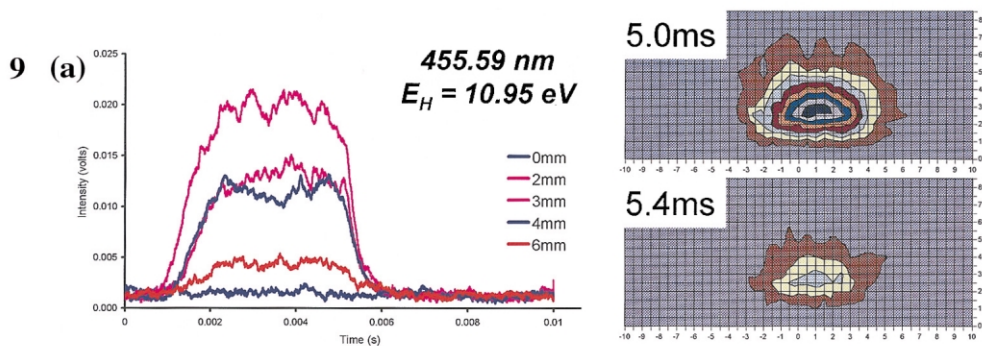
the center of the population maximum moving from 2.5 to 5.5 mm from the cathode surface. This shift in spatial position occurs with a reduction in intensity to 30–40% from the temporal maximum. Emission from the  $3d^{10}6d$  (7.18 eV) electronic state, however, demonstrates opposite behavior. Between 5.1 and 5.5 ms, emission originating from this electronic state increases in both area and intensity reaching 90–100% of its temporal maximum. This temporal maximum is located 6 mm above the cathode surface and radiates outward in all directions. Absorbance measurements show no considerable movement of the copper atom ground state population during this time. The relative shifts of these electronic transitions and changes in intensity must be attributed to changes in excitation processes.

The shift in the emission from  $3d^{10}4p$  (3.82 eV) electronic state can be explained by the radiative decay of higher electronic states, such as the  $3d^{10}6d$  (7.18 eV) state, cascading to populate this level. Excitation to the  $3d^{10}6d$  (7.18 eV) state during the afterpeak time regime arises from recombination of copper ions with thermal electrons producing highly excited copper atoms. The spatial and temporal position at which this population maximizes matches metastable argon maps that have been previously produced in this laboratory [9]. Metastable argon atoms are produced through a similar process where argon ions recombined with thermal electrons. Once formed, metastable argon atoms may lead to an increase in the copper ion ground state through Penning ionization. The afterpeak intensity of the  $3d^{10}6d$  (7.18 eV) continues to 5.6 ms and begins to collapse over the next 1.0 ms. The position of the collapse is localized at approximately 6 mm and does not demonstrate any shift caused by atom diffusion.

Fig. 5 Two-dimensional absorbance maps of the copper atom population monitored through out the pulse cycle using hollow cathode emission at 324.75 nm.

Fig. 6. Two-dimensional maps of a low-lying atom electronic state 3.82 eV above the ground state, monitored by emission at 324.75 nm, throughout the pulse cycle.

Fig. 7. Two-dimensional maps of a high lying atom electronic state 7.18 eV above the ground state, monitored by emission at 368.74 nm, throughout the pulse cycle.



Figs. 9 and 10.

## 5. Classification of copper ion electronic states

An assignment of the copper ion lines was carried out in a similar manner as the copper atom transitions. The highest energy state that was observed occurred 10.99 eV above the ion ground state. All transitions exhibit emissions only during the plateau time regime, that is none demonstrate the afterpeak characteristic observed in atom transitions. These results conflict with previous reports from this laboratory, by which copper ion emissions were mistakenly assigned [3]. Of the observed transitions the 224.70-nm shows unique behavior when compared with all other electronic transitions collected and will be discussed separately. Generalizations regarding the remaining electronic states are inferred from the two electronic regions depicted in the energy level diagram illustrated in Fig. 8. The subsequent emissions originating from these two electronic states are depicted in Fig. 9 and represent emission behavior over different spatial regions in the negative glow. Each transition reaches the steady state, plateau, intensity within 2.0–3.0 ms into the pulse cycle. The relative position for each maximum depends once again on the high-energy electronic level of the transition.

The high-energy state,  $3d^84s^2$ , occurs 10.95 eV above the ion ground state and is monitored by emission at 455.59 nm (Fig. 9A). The behavior of this line is indicative of the other  $3d^84s$  transitions. The adjacent map, 5.0 ms into the pulse cycle, demonstrates a discrete maximum 3 mm from the cathode surface. This spatial distance overlaps well with argon ion emission measurements made in this laboratory [18]. The processes most likely to populate these levels involve ionization followed by electron excitation. This two-step process explains the absence of any ion emission in the afterpeak because electron excitation processes have stopped. Previous reports on

metastable argon atom populations during the plateau and steady state plasmas indicate a large population of metastables within 1–2 mm of the cathode's surface. In this report, electron excitation of copper atoms has been deduced to occur at slightly greater distances. It is uncertain, however, to what degree Penning ionization is involved in the ionization of copper atoms in this two-step mechanism. The adjacent temporal map at 5.4 ms demonstrates no appreciable change in spatial position during the plateau and afterpeak time regimes. The  $3d^94p$  levels are characterized (Fig. 9B), by the 213.60-nm transition that occurs 8.52 eV above the ion ground state. The most probable mechanism for populating this level is ionization followed by electron excitation followed by radiative decay from the  $3d^84s$  levels. Each transition from the  $3d^94p$  levels exhibits a broad spatial maximum occurring 1–2 mm from the cathode surface. This indicates that there is no significant diffusion during the afterpeak time regime.

Emission from the 224.70-nm line, originating from the  $3d^94p$  level (8.23 eV), exhibits a different behavior from that of any other copper ion electronic state studied (Fig. 10). The mechanism and characterization of this transition has been reported previously as charge transfer between a metastable argon ion,  $3p^5\ ^2P_{3/2}$  (15.76 eV), and ground state copper atom [19,20]. This process is very selective because the energy deficit between these two species is only  $\Delta E = -0.02$  eV. It is important to note that emission at 229.40 nm,  $3d^94p$  (8.23 eV), was not observed. The spatial maximum of the 224.70-nm emission occurs 5 mm from the cathode surface at 5.0 ms into the pulse cycle. Unlike any atom or ion temporal profiles collected previously, the emission intensity during the 5.0-ms power pulse never reaches a steady state value. Because copper atom absorbance maps have demonstrated a steady state ground

---

Fig. 9. The temporal emission profiles of copper atom transitions as depicted in Fig. 8, labeled A and B. Each transition demonstrates the change in the temporal emission profile moving vertically from the cathode surface in increments of 2 mm. Adjacent to each are a two-dimensional emission map taken at 5.0 and 5.4 ms.

Fig. 10. The temporal emission profiles of copper ion emission monitored at 224.70 nm as a function of increasing distance, with two-dimensional emission maps.

state population in the plasma within 4.0 ms of pulse initiation, the absence of steady state behavior here is attributed to the production of the metastable argon ion,  $3p^5 \ ^2P_{3/2}$  (15.76 eV). No afterpeak behavior was observed for this copper ion transition, as was the case in other copper ion transitions studied. A further investigation of this transition is planned.

## 6. Conclusions

Copper atom and ion emission profiles from a pulsed glow discharge source are presented. All copper atom transitions monitored demonstrate both plateau and afterpeak behavior. During the plateau time regime, population of the various atom electronic states is accomplished primarily by electron excitation. Once power is terminated, population of the various atom electronic states is through radiative decay of highly excited copper atoms originating from the recombination of Penning ionized copper atoms and thermal electrons. The ratio of afterpeak-to-plateau intensity for the various copper atom transitions was found to increase as a function of the upper energy state of monitored transition. This ratio also suggests an electron excitation temperature equivalent to 5.78 eV during the plateau time regime. Two-dimensional emission maps of different copper atom transitions were presented throughout the pulse cycle. These maps demonstrate relative temporal and spatial positions where electron excitation and Penning ionization dominate. Copper ion emission profiles exhibit only plateau behavior. The most probable mechanism for excitation to these electronic states, excluding 224.70 nm, originated with or included electron excitation. The emission monitored by the 224.70 nm line was found to be very intense and characteristically different, in that it did not reach a plateau intensity, than any other transition monitored. Because no afterpeak was observed for this transition it can be deduced that charge exchange does not play substantial role in the formation of copper ions during the afterpeak time regime.

## Acknowledgements

We thank Professor. H.O. Finklea, Dr Dmitri Brevnov, and Maria Rosa Valero Aracama for their help in writing a Visual Basic program that removes rc time constant distortion. Partial support of this work by the US Department of Energy, DE-FG02-00ER45837, is gratefully acknowledged.

## References

- [1] J.A. Klingler, P.J. Savickas, W.W. Harrison, The pulsed glow discharge as an elemental ion source, *J. Am. Soc. Mass. Spectrom.* 1 (1990) 138–143.
- [2] W. Hang, W.O. Walden, W.W. Harrison, Microsecond pulsed glow discharge as an analytical spectroscopic source, *Anal. Chem.* 68 (1996) 1148–1152.
- [3] F.L. King, C. Pan, Temporal signal profiles of analytical species in modulated glow discharge plasmas, *Anal. Chem.* 65 (1993) 735–739.
- [4] J.A. Klingler, C.M. Barshick, W.W. Harrison, Factors influencing ion signal profiles in pulsed glow discharge mass spectrometry, *Anal. Chem.* 63 (1991) 2571–2576.
- [5] C.L. Lewis, E.S. Oxley, C. Pan, R.E. Steiner, F.L. King, Determination of  $^{40}\text{Ca}^+$  in the presence of  $^{40}\text{Ar}^+$ : an illustration of the utility of time gated detection in pulsed glow discharge mass spectrometry, *Anal. Chem.* 71 (1999) 230–234.
- [6] V. Majidi, M. Moser, C. Lewis, W. Hang, F.L. King, Explicit chemical speciation by microsecond pulsed glow discharge time-of-flight mass spectrometry: concurrent acquisition of structural, molecular, and elemental information, *J. Anal. At. Spectrom.* 15 (2000) 19–25.
- [7] F.L. King, J. Teng, R.E. Steiner, Glow discharge mass spectrometry: trace element determinations in solid samples, *J. Mass. Spectrom.* 30 (1995) 1061–1065.
- [8] R.L. Smith, D. Serxner, K.R. Hess, Assessment of the relative role of Penning ionization in low-pressure glow discharges, *Anal. Chem.* 61 (1989) 1103–1108.
- [9] G.P. Jackson, C.L. Lewis, S.K. Doorn, V. Majidi, F.L. King, Spectral, spatial, and temporal characteristics of a millisecond pulsed glow discharge: metastable argon atom production. Manuscript submitted.
- [10] P.A. Janson, *Deconvolution with Applications in Spectroscopy*, Academic Press, Inc, Orlando Florida, 1984.
- [11] A. Bogaerts, R. Gijbels, Behavior of the sputtered copper atoms, ions and excited species in a radio-frequency and direct current glow discharge, *Spectrochim. Acta Part B* 55 (2000) 279–297.
- [12] W.L. Wiese, G.A. Martin, *Wavelengths and Transition Probabilities for Atoms and Atomic Ions*, NSRDS-NBS, 1980.
- [13] B. Chapman, *Glow Discharge Processes, Sputtering and Plasma Etching*, John Wiley and Sons, New York, 1980.

- [14] F.P. Ferreira, H.G.C. Human, A study of the density of sputtered atoms in the plasma of the modified Grimm-type glow discharge source, *Spectrochim. Acta Part B* 36 (1981) 215–229.
- [15] K. Hoppstock, W.W. Harrison, Spatial distribution of atoms in a dc glow discharge, *Anal. Chem.* 67 (1995) 3167–3171.
- [16] A. Bogaerts, E. Wagner, B.W. Smith, J.D. Winefordner, D. Pollman, W.W. Harrison, R. Gijbels, Three-dimensional density profiles of sputtered atoms and ions in a direct current glow discharge: experimental study and comparison with calculations, *Spectrochim. Acta Part B* 52 (1997) 205–218.
- [17] A. Bogaerts, R. Gijbels, Two-dimensional model of a direct current glow discharge: description of the argon metastable atoms, sputtered atoms, and ions, *Anal. Chem.* 68 (1996) 2676–2685.
- [18] G.P. Jackson, C.L. Lewis, F.L. King, Spectral, spatial, and temporal characteristics of a millisecond pulsed glow discharge: argon atom and ion emission. Manuscript in preparation.
- [19] E.B.M. Steers, J.F. Fielding, Charge-transfer excitation processes in the Grimm lamp, *J. Anal. At. Spectrom.* 2 (1987) 239–244.
- [20] K. Wagatsuma, K. Hirokawa, Spectrometric studies of excitation mechanisms on singly-ionized copper emission lines in Grimm-type glow discharge plasmas with helium mixture technique, *Spectrochim. Acta Part B* 46 (1991) 269–281.